Optics & Laser Technology 169 (2024) 110020

Contents lists available at ScienceDirect

Optics and Laser Technology

journal homepage: www.elsevier.com/locate/optlastec

Full length article

Experimental realization of Airy beams on incoherent background

Qian Chen [a,b], Morteza Hajati [c], Xin Liu [a,b,*], Yangjian Cai [a,b,d,**], Sergey A. Ponomarenko [c,e,**], Chunhao Liang [a,b,**]

[a] Shandong Provincial Engineering and Technical Center of Light Manipulations & Shandong Provincial Key Laboratory of Optics and Photonic Device, School of Physics and Electronics, Shandong Normal University, Jinan 250014, China
[b] Collaborative Innovation Center of Light Manipulations and Applications, Shandong Normal University, Jinan 250358, China
[c] Department of Electrical and Computer Engineering, Dalhousie University, Halifax, Nova Scotia, B3J 2X4, Canada
[d] School of Physical Science and Technology, Soochow University, Suzhou 215006, China
[e] Department of Physics and Atmospheric Science, Dalhousie University, Halifax, Nova Scotia, B3H 4R2, Canada

ARTICLE INFO

Keywords:
Airy beam
Structured random light
Self-healing
Non-diffraction

ABSTRACT

We report an experimental realization of recently introduced Airy beams on incoherent background (ABIBs). The ABIBs are structured random beams that defy diffraction in free space, making them attractive to free-space optical communications, information transfer and imaging. We demonstrate here that the (truncated) laboratory realizations of ABIBs are more resilient to diffraction and far more capable of self-healing after having been obstructed by defects than are truncated coherent Airy beams of the same width of the main lobe and truncation length. The combination of remarkable propagation invariance and self-healing potential of ABIBs carries promise for their applications to optical communications in randomly inhomogeneous environments and biological tissue imaging.

1. Introduction

Structuring random light has recently triggered a flurry of research activity [1–7]. Not only do structured random light beams possess tailored (average) intensity distributions and polarization states, just as their coherent cousins [8], but they feature customized spatial and/or temporal field correlations as well. The latter are at the heart of remarkable resilience of structured random light to environmental noise, whether it is caused by turbulence [9,10], or random obstacles/impurities in the medium [11,12].

Although uniformly correlated light beams [13,14], or beam arrays [15,16] have initially received much attention, the potential of non-uniformly correlated light beams for a multitude of optical applications has been slowly recognized [17–28]. The original theoretical work [17] was followed by the experimental realization of non-uniformly correlated beams composed of two [18] and multiple uncorrelated modes [24], as well as by further theoretical [19–21,26,28] and experimental [22,23,25,27] research into structuring non-uniformly correlated light.

In this context, the structured random beams withstanding free-space diffraction have been conjectured to play a special role in optical imaging and communications [29,30]. Instructively, it has been demonstrated theoretically [19] and experimentally [25,31] that propagation-invariant in free space random wave packets necessarily feature non-uniform field correlations as they manifest themselves as bumps/dips residing atop of a statistically uniform pedestal (background). One of the most attractive features of such diffraction-free random beams is their capacity to remain structurally stable on propagation through a statistically homogeneous isotropic random medium, such as the turbulent atmosphere [10].

Recently, it has been theoretically discovered [32] that Airy bumps situated on top of a statistically uniform, Gaussian correlated background (ABIBs) are propagation-invariant in free space. Moreover, their truncated, finite-power versions are robust against diffraction as well. However, ABIBs have not yet been experimentally generated, to our knowledge.

In this Letter, we report a laboratory realization of Airy beams on incoherent background. Further, we demonstrate their resilience

* Corresponding author at: Shandong Provincial Engineering and Technical Center of Light Manipulations & Shandong Provincial Key Laboratory of Optics and Photonic Device, School of Physics and Electronics, Shandong Normal University, Jinan 250014, China.
** Corresponding authors.
E-mail addresses: cnliuxin1995@gmail.com (X. Liu), yangjiancai@sdnu.edu.cn (Y. Cai), serpo@dal.ca (S.A. Ponomarenko), chunhaoliang@sdnu.edu.cn (C. Liang).

https://doi.org/10.1016/j.optlastec.2023.110020
Received 27 May 2023; Received in revised form 17 August 2023; Accepted 1 September 2023

to diffraction and capacity to self-heal after they encounter opaque obstacles. Notably, we show that the ABIB resilience to free-space diffraction and, especially, self-healing capacity are superior to those of truncated coherent Airy beams of the same width of the main lobe and truncation length. The superb resistance to diffraction and scattering by opaque obstacles makes the ABIBs attractive for optical imaging and information transfer through random environments.

2. Theroy

We start by recalling that the average intensity distribution of an ideal isotropic ABIB source reads [32]

$$I(\mathbf{r}) \propto 1 + P_{2D} e^{\xi_c^3/6} \prod_{j=x,y} \exp\left(\frac{\sigma_c^2 r_j}{2\sigma_I^3}\right) \mathrm{Ai}\left(\frac{r_j + \xi_c^2 \sigma_I/4}{\sigma_I}\right). \tag{1}$$

Here $P_{2D} = 2\pi\xi_c$ is a dimensionless power carried by an Airy bump $\mathrm{Ai}(x)$ residing atop a statistically uniform pedestal and $\xi_c = \sigma_c^2/\sigma_I^2$ is a coherence parameter, with σ_c and σ_I standing for the transverse coherence length of the pedestal (background) and the width of the Airy bump, respectively. Further, $\mathbf{r} = (r_x, r_y)$ is a two-dimensional radius vector in the source plane. We remark that both the amount of power contained in the bump and the truncation width $w_t = \sigma_I^3/\sigma_c^2$ of the bump profile are completely determined by σ_c and σ_I.

Next, we can express the cross-spectral density of an isotropic ABIB source as [32]

$$W(\mathbf{r}_1, \mathbf{r}_2) = \int p(\mathbf{k}) \mathscr{A}^*(\mathbf{k}, \mathbf{r}_1) \mathscr{A}(\mathbf{k}, \mathbf{r}_2) d^2\mathbf{k}, \tag{2}$$

where a (nonnegative) spectral power density $p(\mathbf{k})$ has a Gaussian profile as

$$p(\mathbf{k}) = \frac{\sigma_c}{\sqrt{2\pi}} \exp\left(-\frac{\sigma_c^2 \mathbf{k}^2}{2}\right), \tag{3}$$

and a chirped plane wave profile $\mathscr{A}(\mathbf{k}, \mathbf{r})$ is given by the expression

$$\mathscr{A}(\mathbf{k}, \mathbf{r}) \propto \cos\left[\frac{1}{6}\sigma_I^3(k_x^3 + k_y^3) + \frac{1}{2a}\mathbf{k} \cdot \mathbf{r}\right]. \tag{4}$$

Here a is a dimensionless constant controlling the stripe spacing of a cosine function in our experiment and $\mathbf{k} = (k_x, k_y)$ is a 2D radius vector in the reciprocal space. We notice that introducing the stripe spacing into our experimental protocol implies rescaling all transverse coordinates in Eq. (1) as $\mathbf{r} \to \mathbf{r}/a$, and hence rescaling the Airy bump width to $a\sigma_I$.

Considering statistical inhomogeneity of ABIBs, we cannot generate them in the laboratory with the aid of a rotating ground-glass diffuser [5,14,33] We then employ a pseudo-mode superposition principle [2,5,34–37] to construct the ABIBs by discretizing Eqs. (2) through (4) to yield

$$W(\mathbf{r}_1, \mathbf{r}_2) \simeq \sum_{m,n} p(\mathbf{k}_{mn}) \mathscr{A}^*(\mathbf{k}_{mn}, \mathbf{r}_1) \mathscr{A}(\mathbf{k}_{mn}, \mathbf{r}_2). \tag{5}$$

Here $\mathbf{k}_{mn}$ is evaluated at discrete locations labeled by the indices m and n across the entire reciprocal plane. Next, $p(\mathbf{k}_{mn})$ and $\mathscr{A}(\mathbf{k}_{mn}, \mathbf{r})$ are the mode weight and discrete pseudo-mode profile, respectively. In agreement with the previous work [14], the smaller the area under the distribution $p(\mathbf{k})$, the smaller the required number of pseudo-modes, which, in turn, implies higher coherence of the source.

To realize the ABIBs in the laboratory, we must first generate each pseudo-mode, followed by superposing appropriately normalized pseudo-modes. To this end, we can write the electric field of an individual mode as $U_{mn}(\mathbf{r}) = \sqrt{p(\mathbf{k}_{mn})}\mathscr{A}(\mathbf{k}_{mn}, \mathbf{r})$. In the experiment, the pseudo-modes are produced by illuminating a phase-only spatial light modulator (SLM), preloaded with customized phase gratings, with a plane wave. We follow the complex amplitude modulation encoding algorithm [38] to customize the gratings. The SLM phase is then given by

$$\phi_{SLM}(\mathbf{r}) = A \sin\left\{\mathrm{Arg}\left[U_{mn}(\mathbf{r})\right] + 2\pi f_x x\right\}. \tag{6}$$

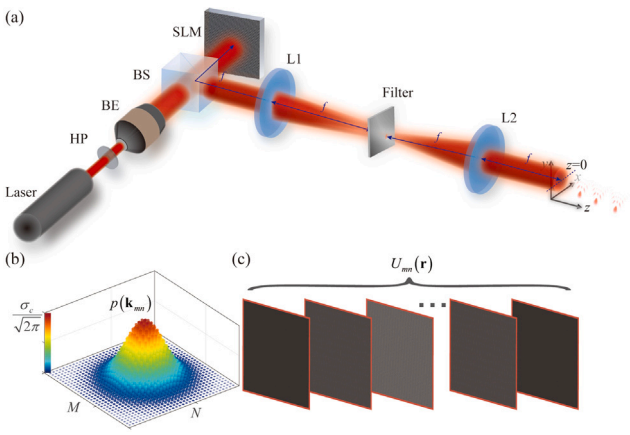

Fig. 1. (a) Experimental setup for ABIB generation; (b) discretized modal weight distribution $p(\mathbf{k}_{mn})$; (c) random ensemble of phase gratings loaded onto the SLM. HP: half-wave plate; BE: beam expander; BS: beam splitter; L1, L2: identical lenses of focal length $f = 250$ mm; Filter: a circular aperture.

Here "Arg" stands for the principal value of the (random) phase of the field; A is obtained via numerical inversion: $J_1(A) = |U_{mn}|$, where J_1 denotes a Bessel function of the first kind and first order. Further, the phase shift $2\pi f_x x$ is imposed by a blazed grating, where f_x denotes an inverse spatial period of the grating.

We sketch our experimental setup in Fig. 1. A fully coherent, linearly polarized beam with the wavelength $\lambda = 632.8$ nm, emitted by a He–Ne laser, is transmitted through a half wave plate (HP) and expanded by a beam expander (BE). Here, the HP rotates the polarization direction of the incident beam to obtain a horizontally polarized output since the SLM only responds to the latter. The resulting beam passes through a beam splitter (BS) and illuminates the SLM. We load the phase gratings generated by Eq. (6) onto the SLM. The beam, reflected by the SLM and BS, is then transmitted through a 4f-optical imaging system composed of the lenses L1, L2 and a filter. We place a circular aperture as a filter in the Fourier spectrum plane of L2 to filter out a positive or negative first-order diffraction output of the grating, which is our desired output. We refresh the gratings, loaded onto the SLM [see Fig. 1(c)], to generate a statistical ensemble of individual modes. We then synthesize the cross-spectral density of the ABIB with the help of Eq. (5). The average ABIB intensity is $I(\mathbf{r}) = W(\mathbf{r}, \mathbf{r}) \simeq \sum_{m,n} |U_{mn}(\mathbf{r})|^2$. We note that the pseudo-modes, comprising the ABIB source, are truncated by the SLM screen in our experiment.

First of all, we present our experimental reconstruction of an ABIB source and compare our results with the theory. The numerical and experimental ABIB source realizations are exhibited in the top and middle rows of Fig. 2, respectively, for different values of σ_c. Further, we display the numerically simulated (solid) and experimental (dotted) average intensity profiles $I(x, y = y_p)$ of the ABIB, where y_p denotes the y-coordinate of the peak ABIB intensity, in the bottom row of Fig. 2. In our numerical simulations, we utilize truncated modes with the truncation aperture equal to the SLM screen area to ensure a fair comparison of the experiment with simulations. We observe excellent agreement between our simulations and our experimental source reconstruction to the point that numerical (solid blue) and experimental (dotted red) curves nearly coincide. Instructively, our experimental results indicate that the ABIB tail elongates as the pedestal coherence length decreases. This is consistent with the ABIB theory as the characteristic truncation width of the Airy bump is inversely proportional to the square of said coherence length, $w_t \propto \sigma_c^{-2}$, cf., Eq. (1).

Next, we explore free-space propagation properties of the beams generated by experimentally realized ABIB sources and compare the results with numerical simulations. In our numerical work, we propagate individual modes from the source to a receiver plane one by

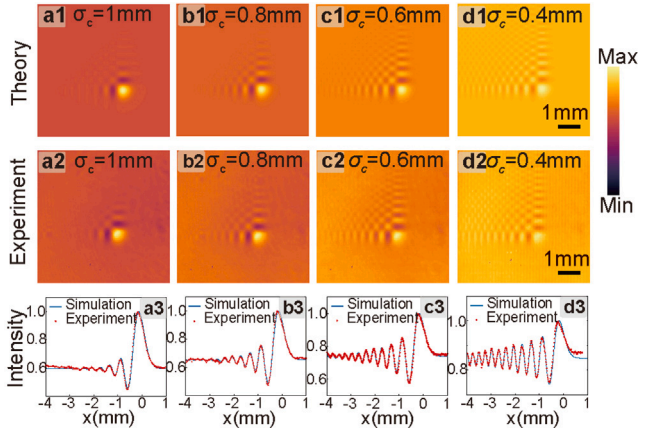

Fig. 2. (a1)–(d1) Theoretical and (a2)–(d2) experimental 2D average intensity profiles of an ABIB with $\sigma_I = 1.2$ mm at the source; the magnitude of σ_c is indicated in each panel. (a3)–(d3) Theoretical (solid blue) and experimental (dotted red) 1D average intensity distribution $I\left(x, y = y_p\right)$ curves, where y_p denotes the y-coordinate of the peak intensity of the ABIB source. The number of the adopted modes from the left column to the right column are 3600, 10,000, 10,000 and 40,000 respectively.

one, which can be achieved via the convolution between the source mode with the impulse response function of free-space [2]. The ABIB intensity then follows from the mode superposition, Eq. (5), by letting $\mathbf{r}_1 = \mathbf{r}_2 = \mathbf{r}$. We show our numerical and experimental results in the top and middle rows of Fig. 3. The theoretical (blue solid) and experimental (red dotted) curves, displayed in the bottom row of the figure, yield the average intensity distributions $I\left(x, y = y_p\right)$ evaluated at the y-coordinate y_p of the peak intensity of the ABIB. The experiment and numerics are in excellent agreement. The overall color difference of the panels in the top and middle rows is mainly due to noise, whereas small intensity fluctuations stem from a finite number of modes employed to synthesize the ABIB source. It is instructive to compare the ABIB resilience to diffraction to that of a coherent Airy beam. To this end, we consider the electric field envelope profile Ψ of a truncated Airy beam [39] with the same main lobe width and truncation length as those of our experimentally generated ABIB at the source, i.e.,

$$\Psi(x) \propto \mathrm{Ai}\left(\frac{x}{a\sigma_I}\right) \exp\left(\frac{\xi_c}{4}\frac{x}{a\sigma_I}\right), \tag{7}$$

with $\sigma_I = 1.2$ mm, $a = 0.15$ and $\xi_c = 4/9$. We display free-space evolution of $|\Psi|^2$ in Fig. 4. We can infer from the figure that not only does the Airy beam spread quite a bit, but its structure is also altered on propagation. Specifically, the Airy profile acquires a rather long tail, and the contrast of its side lobes gradually decreases away from the main lobe [see Fig. 4(c)]. At the same time, the Airy structure of the ABIB of the same width of the main lobe and truncation length remains nearly intact at this distance, as is evidenced by Fig. 3 (c1) and (c2).

Last, we explore the ABIB self-healing capacity. We take an inverted Gaussian filter as a model of an obstacle and place it in the source plane for simplicity. The obstacle transmittance function is $T(\mathbf{r}) = 1 - \exp(-\mathbf{r}^2/R^2)$, where R denotes the transverse width of the obstacle. We exhibit our numerical and experimental results in the top and bottom rows of Fig. 5. We mark the obstacle position with a white dotted circle. It follows from the figure that although the main lobe of the Airy bump is initially blocked by the obstacle [see Fig. 5. (a1)], the energy gradually flows from the side lobes back to the main lobe [see Fig. 5. (b1) and (c1)], prompting the latter to reconstruct [see Fig. 5. (d1)]. The structure of the recovered ABIB [see Fig. 5. (d1)] is consistent with that of the ABIB source [see Fig. 3. (a1)]. Once again, we find excellent agreement between our experimental results and our simulations, cf., top and bottom rows of Fig. 5.

To illustrate superb ABIB self-healing capacity, we compare the self-healing dynamics of an ABIB with that of the truncated coherent

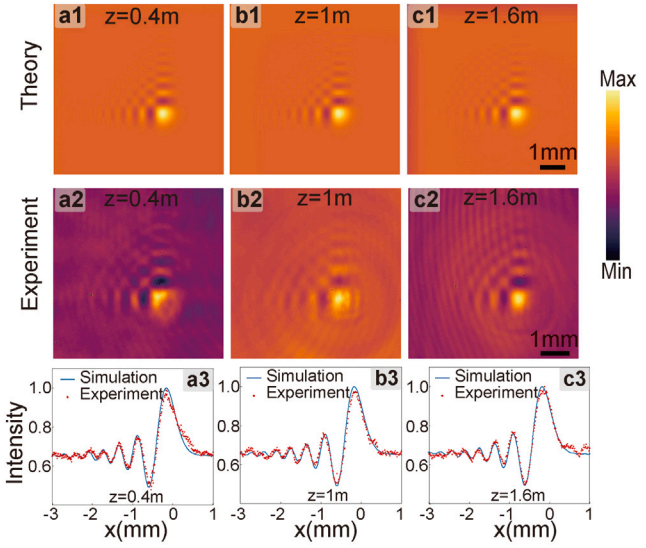

Fig. 3. (a1)–(c1) Theoretical and (a2)–(c2) experimental 2D average intensity plots of an ABIB with $\sigma_I = 1.2$ mm and $\sigma_c = 0.8$ mm propagating in free space from the source to a receiver plane; the propagation distance z is indicated in each panel. (a3)–(c3) The theoretical (solid blue) and experimental (dotted red) 1D average intensity distribution $I\left(x, y = y_p\right)$ curves, where y_p denotes the y-coordinate of the peak intensity of the ABIB source.

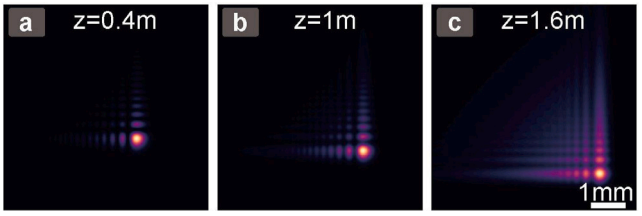

Fig. 4. Evolution of the intensity of a truncated fully coherent Airy beam in free space. The main lobe width of the beam is $a\sigma_I$ with $\sigma_I = 1.2$ mm and $a = 0.15$. The transverse truncation length of the beam equals to that of the ABIB with the same main lobe width and coherence parameter $\xi_c = 4/9$.

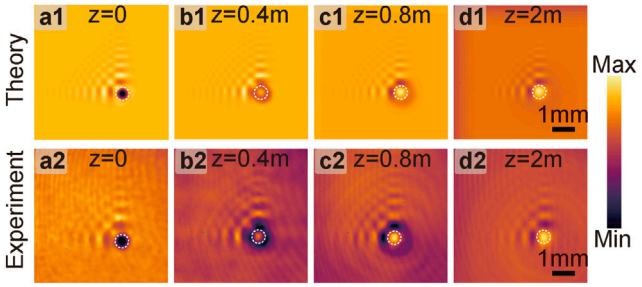

Fig. 5. (a1)–(d1) Numerical and (a2)–(d2) experimental results for the evolution of a partially obstructed ABIB with $\sigma_I = 1.2$ mm and $\sigma_c = 0.8$ mm in free space. The transverse width of the obstacle is R = 0.2 mm.

Airy beam with the same main lobe width and truncation length. The spatial profile of the latter is given by Eq. (7) with $\sigma_I = 1.2$ mm and $\sigma_c = 0.8$ mm. We assume an obstacle blocks half of the main lobe cross-section of either beam at the source. To quantify self-healing capacity, we employ a self-healing similarity degree index (SDI) defined as [12]

$$\mathrm{SDI}(z) = \frac{\left[\iint I_{ob}(\mathbf{r}, z)\, I_{nob}(\mathbf{r}, z)\, d^2\mathbf{r}\right]^2}{\iint I_{ob}^2(\mathbf{r}, z)\, d^2\mathbf{r} \iint I_{nob}^2(\mathbf{r}, z)\, d^2\mathbf{r}}, \tag{8}$$

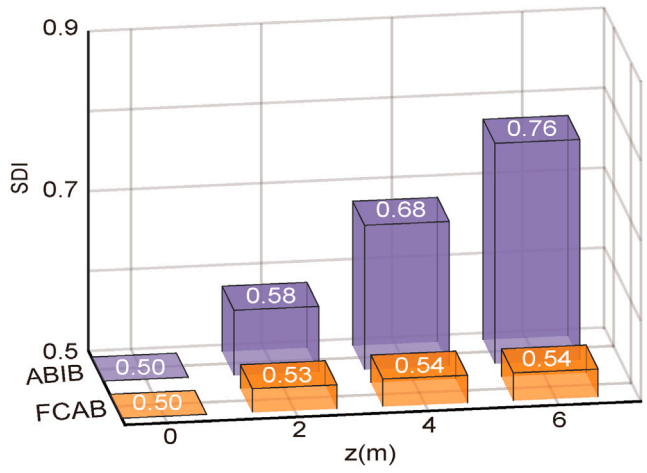

Fig. 6. Free-space SDI evolution of a truncated coherent Airy beam (FCAB) and the ABIB with σ_I = 1.2 mm and σ_c = 0.8mm, blocked by an obstacle at the source. The obstacle is the same as that in Fig. 5 and the coherent Airy beam has the same main lobe and truncation widths as the ABIB.

where I_{ob} and I_{nob} denote the average intensities of ABIB with and without obstruction, respectively. The SDI falls within the range $[0, 1]$; the greater the SDI, the better the self-healing capacity. We plot the evaluated SDIs in Fig. 6. The orange and violet bars correspond to the coherent Airy beam and the ABIB, respectively. The SDI attains the value of 0.5 at the source in both cases, as half of either beam cross-section is blocked at the outset. As the propagation distance increases, the SDI of the fully coherent Airy beam barely grows, quickly saturating at around 0.54. It follows that the Airy beam capacity to self-heal is rather limited. At the same time, the ABIB SDI attains the value of 0.76 at z = 6 m. We can then conclude that an ABIB has far superior self-healing capacity to a coherent Airy beam of the same main lobe width and truncation length.

3. Conclusion

In conclusion, we have advanced a protocol to experimentally realize recently introduced Airy beams on incoherent background. To this end, we have structured phase gratings to generate pseudo-modes with the aid of the complex amplitude encoding algorithm; an ensemble of modes is generated by refreshing the gratings on the SLM screen. Hence, the synthesis time is mainly limited by the refresh rate of the SLM. The time could be much saved by adopting other optical device with higher refresh rate, such as digital micromirrors device (typical up to 17 KHz). We have then superposed the appropriately normalized uncorrelated modes to realize an ABIB source. Our experimental results are in excellent agreement with the theory of ABIBs and our numerical simulations. In this manuscript, the prominent advantage of the adopted pseudo mode method is that the arbitrary genuine partially coherent beams can be faithfully constructed. On a different note, the beams generated by this method do not obey Gaussian statistics, so the optical coherence of the beams cannot be measured through classical Hanbury Brown–Twiss method [5]. We have demonstrated that the ABIBs have superior resilience to diffraction and self-healing capacity to conventional coherent Airy beams of the same main lobe width and truncation length. Our work opens up new avenues for exploring the potential of structured random Airy beams. Specifically, the combination of remarkable propagation invariance and self-healing potential of ABIBs carries promise for their applications to optical communications and imaging in randomly inhomogeneous environments.

Funding

This research was funded by National Key Research and Development Program of China (Grant Nos. 2022YFA1404800 and 2019YFA0705000); National Natural Science Foundation of China (Grant Nos. 12004220, 11974218, 12192254, and 92250304); Qingchuang Science and Technology Plan of Shandong Province (Grant No. 2022KJ246); China Postdoctoral Science Foundation (Grant No. 2022T150392); Natural Sciences and Engineering Research Council of Canada (Grant No. RGPIN-2018-05497).

CRediT authorship contribution statement

Qian Chen: Data curation, Visualization, Formal analysis, Writing – original draft. **Morteza Hajati:** Formal analysis, Investigation. **Xin Liu:** Methodology, Investigation. **Yangjian Cai:** Conceptualization, Funding acquisition, Supervision. **Sergey A. Ponomarenko:** Conceptualization, Writing – review & editing, Supervision, Funding acquisition. **Chunhao Liang:** Conceptualization, Writing – review & editing, Supervision, Funding acquisition.

Declaration of competing interest

The authors declare that they have no known competing financial interests or personal relationships that could have appeared to influence the work reported in this paper.

Data availability

Data will be made available on request

References

[1] D. Peng, Z. Huang, Y. Liu, Y. Chen, et al., Optical coherence encryption with structured random light, PhotoniX 2 (2021) 1–15.
[2] Y. Shen, H. Sun, D. Peng, Y. Chen, et al., Optical image reconstruction in 4 f imaging system: Role of spatial coherence structure engineering, Appl. Phys. Lett. 118 (2021) 181102.
[3] L. Liu, W. Liu, F. Wang, H. Cheng, et al., Spatial coherence manipulation on the disorder-engineered statistical photonic platform, Nano Lett. 22 (2022) 6342–6349.
[4] X. Liu, S.A. Ponomarenko, F. Wang, Y. Cai, et al., Incoherent mode division multiplexing for high-security information encryption, 2023, arXiv, preprint arXiv:2304.06455.
[5] X. Liu, Q. Chen, J. Zeng, Y. Cai, et al., Measurement of optical coherence structures of random optical fields using generalized Arago spot experiment, Opto-Electron. Sci. 2 (2023) 220024-1.
[6] C. Liang, F. Wang, X. Liu, Y. Cai, O. Korotkova, Experimental generation of cosine-Gaussian-correlated Schell-model beams with rectangular symmetry, Opt. Lett. 39 (2014) 769–772.
[7] Y. Cai, Y. Chen, J. Yu, X. Liu, L. Liu, Generation of partially coherent beams, Prog. Opt. 62 (2017) 157–223.
[8] A. Forbes, M. de, Oliveira, M.R. Dennis, Structured light, Nature Photon. 15 (2021) 253–262.
[9] G. Gbur, Partially coherent beam propagation in atmospheric turbulence, J. Opt. Soc. Amer. A 31 (2014) 2038–2045.
[10] Z. Xu, X. Liu, Y. Cai, S.A. Ponomarenko, et al., Structurally stable beams in the turbulent atmosphere: dark and antidark beams on incoherent background, J. Opt. Soc. Amer. A 39 (2022) C51–C57.
[11] F. Wang, Y. Chen, X. Liu, Y. Cai, et al., Self-reconstruction of partially coherent light beams scattered by opaque obstacles, Opt. Express 24 (2016) 23735–23746.
[12] Z. Xu, X. Liu, Y. Chen, F. Wang, et al., Self-healing properties of Hermite-Gaussian correlated Schell-model beams, Opt. Express 28 (2020) 2828–2837.
[13] L. Mandel, E. Wolf, Optical Coherence and Quantum Optics, Cambridge university Press, 1995.
[14] Y. Cai, Y. Chen, F. Wang, Generation and propagation of partially coherent beams with nonconventional correlation functions: a review, J. Opt. Soc. Amer. A 31 (2014) 2083–2096.
[15] C. Liang, X. Zhu, C. Mi, X. Peng, et al., High-quality partially coherent Bessel beam array generation, Opt. Lett. 43 (2018) 3188–3191.
[16] H. Mao, Y. Chen, C. Liang, L. Chen, et al., Self-steering partially coherent vector beams, Opt. Express 27 (2019) 14353–14368.

[17] S.A. Ponomarenko, A class of partially coherent beams carrying optical vortices, J. Opt. Soc. Amer. A 18 (2001) 150–156.
[18] G.V. Bogatyryova, C.V. Felde, P.V. Polyanskii, S.A. Ponomarenko, et al., Partially coherent vortex beams with a separable phase, Opt. Lett. 28 (2003) 878–880.
[19] S.A. Ponomarenko, W. Huang, M. Cada, Dark and antidark diffraction-free beams, Opt. Lett. 32 (2007) 2508–2510.
[20] R. Borghi, F. Gori, S.A. Ponomarenko, On a class of electromagnetic diffraction-free beams, J. Opt. Soc. Amer. A 26 (2009) 2275–2281.
[21] H. Lajunen, T. Saastamoinen, Propagation characteristics of partially coherent beams with spatially varying correlations, Opt. Lett. 36 (2011) 4104–4106.
[22] M.W. Hyde IV, S.R. Bose-Pillai, R.A. Wood, Synthesis of non-uniformly correlated partially coherent sources using a deformable mirror, Appl. Phys. Lett. 111 (2017) 101106.
[23] A.S. Ostrovsky, J. Garcia-Garcia, C. Rickenstorff-Parrao, M.A. Olvera-Santamaria, Partially coherent diffraction-free vortex beams with a Bessel-mode structure, Opt. Lett. 42 (2017) 5182–5185.
[24] X. Chen, J. Li, S.M.H. Rafsanjani, O. Korotkova, Synthesis of Im-Bessel correlated beams via coherent modes, Opt. Lett. 43 (2018) 3590–3593.
[25] X. Zhu, F. Wang, C. Zhao, Y. Cai, et al., Experimental realization of dark and antidark diffraction-free beams, Opt. Lett. 44 (2019) 2260–2263.
[26] M.W. Hyde, S. Avramov-Zamurovic, Generating dark and antidark beams using the genuine cross-spectral density function criterion, J. Opt. Soc. Amer. A 36 (2019) 1058–1063.
[27] Y. Liu, Y. Chen, F. Wang, Y. Cai, et al., Robust far-field imaging by spatial coherence engineering, Opto-Electron. Adv. 4 (2021) 210027.
[28] D. Raveh, O. Korotkova, Coherence–orbital angular momentum matrix of non-uniformly correlated sources, Opt. Lett. 47 (2022) 5719–5722.
[29] J. Turunen, A. Vasara, A.T. Friberg, Propagation invariance and self-imaging in variable-coherence optics, J. Opt. Soc. Amer. A 8 (1991) 282–289.
[30] J. Turunen, A.T. Friberg, Propagation-invariant optical fields, Prog. Opt. 54 (2010) 1–88.
[31] M. Yessenov, B. Bhaduri, H.E. Kondakci, M. Meem, et al., Non-diffracting broadband incoherent space–time fields, Optica 6 (2019) 598–607.
[32] M. Hajati, V. Sieben, S.A. Ponomarenko, Airy beams on incoherent background, Opt. Lett. 46 (2021) 3961–3964.
[33] F. Wang, H. Lv, Y. Chen, Y. Cai, et al., Three modal decompositions of Gaussian Schell-model sources: comparative analysis, Opt. Express 29 (2021) 29676–29689.
[34] F. Gori, M. Santarsiero, Devising genuine spatial correlation functions, Opt. Lett. 32 (2007) 3531–3533.
[35] S.A. Ponomarenko, Complex Gaussian representation of statistical pulses, Opt. Express 19 (2011) 17086–17091.
[36] D. Voelz, X.F. Xiao, O. Korotkova, Numerical modeling of schell-model beams with arbitrary far-field patterns, Opt. Lett. 40 (2015) 352–355.
[37] S. Zhu, P. Li, Z.H. Li, Y. Cai, et al., Generating non-uniformly correlated twisted sources, Opt. Lett. 46 (2021) 5100–5103.
[38] C. Rosales-Guzmán, A. Forbes, How to Shape Light with Spatial Light Modulators, SPIE, 2017.
[39] G.A. Siviloglou, J. Broky, A. Dogariu, D.N. Christodoulides, Observation of accelerating Airy beams, Phys. Rev. Lett. 99 (2007) 213901.